Pergamon

Geochimica et Cosmochimica Acta, Vol. 65, No. 20, pp. 3491–3503, 2001

0016-7037/01 $20.00 + .00

PII S0016-7037(01)00647-0

Coprecipitation of Uranium(VI) with Calcite: XAFS, micro-XAS, and luminescence characterization

RICHARD J. REEDER,[1,*] MELISSA NUGENT,[1] C. DREW TAIT,[2] DAVID E. MORRIS,[2] STEVE M. HEALD,[3] KENNETH M. BECK,[3] WAYNE P. HESS,[3] and ANTHONY LANZIROTTI[4]

[1]Department of Geosciences, State University of New York at Stony Brook, Stony Brook, NY 11794-2100, USA
[2]Chemistry Division and Seaborg Institute for Transactinium Science, Los Alamos National Laboratory, Los Alamos, NM 87545, USA
[3]Environmental Molecular Science Laboratory, Pacific Northwest National Laboratory, Richland, WA 99352, USA
[4]Consortium for Advanced Radiation Sources, University of Chicago, Chicago, IL, USA

(*Received December* 11, 2000; *accepted in revised form April* 6, 2001)

Abstract—X-ray absorption and luminescence spectroscopies have been used to characterize the local structure and coordination of uranium(VI) species coprecipitated with calcite ($CaCO_3$) from room-temperature aqueous solutions. Different solution chemistries and pHs are found to result in differences in the equatorial coordination of the uranyl species (UO_2^{2+}) incorporated in the calcite, with multiple coordination environments of uranyl evident in one sample. Differences in the equatorial coordination between the aqueous uranyl species and those found in the calcite indicate that coordination changes occur during incorporation of at least some species. This contrasts with previous findings showing no change in equatorial coordination during uranyl incorporation into aragonite, and may explain the greater incorporation in this latter phase. The absence of calcium backscatterers and well defined structure beyond the equatorial shell is consistent with disorder associated with disruption of the local calcite structure. This may indicate an inability of the uranyl unit to assume a stable structural environment in the host calcite, which could decrease the stability of uranyl-containing calcite.

Calcite single crystals grown in uranyl-containing solutions exhibit polygonized spiral growth hillocks on $(10\bar{1}4)$ surfaces composed of four vicinal surfaces, consistent with face symmetry. Micro-X-ray fluorescence reveals that uranium is differentially incorporated between nonequivalent vicinal surfaces, reflecting step-selective incorporation of uranyl species during growth. Micro-X-ray absorption near-edge structure spectra from the nonequivalent vicinal faces fail to reveal any differences in speciation between the vicinals or that might account for the presence of the multiple coordination environments identified by luminescence and X-ray absorption spectroscopies. *Copyright © 2001 Elsevier Science Ltd*

1. INTRODUCTION

The uptake of U(VI) during the crystallization of calcite represents a potentially important process affecting the mobility and sequestration of this radionuclide in the near surface environment. Several experimental studies have addressed mechanisms of U(VI) uptake by calcite, including adsorption and coprecipitation (Carroll et al., 1992; Meece and Benninger, 1993; Geipel et al., 1997; Reeder et al., 2000). More generally, the mechanisms of metal uptake by calcite have been the subject of extensive study (e.g., Davis et al., 1987; Mucci and Morse, 1990; Zachara et al., 1991; Stipp et al., 1992; Xu et al., 1996; Sturchio et al., 1997; Rimstidt et al., 1998; Curti, 1999; Cheng et al., 2000). An important view emerging from this body of work is that coprecipitation and formation of a solid solution are likely to be the dominant mechanisms of metal uptake by carbonates over time scales relevant for environmental contaminants. Evaluating the effectiveness of this process for sequestration and the potential for remobilization requires an understanding of how metal contaminants are bound with the calcite.

U(VI) occurs principally as the linear uranyl moiety (O=U=O), which may be highly soluble and mobile in conditions characteristic of many surface waters. The formation of stable complexes with CO_3^{2-} enhances U(VI) solubility in carbonate-containing solutions and is the basis for some remediation techniques. In contrast, U(IV) shows limited mobility owing to its very low solubility. Although experimental studies of U(VI) coprecipitation with calcite suggest partition coefficients less than one (Kitano and Oomori, 1971; Meece and Benninger, 1993), significant solid uranium concentrations have nevertheless been reported for calcite growth in laboratory time scales (Reeder et al., 2000). Rapid calcification may be important during interaction of highly alkaline wastes with vadose zone materials and also during natural pedogenesis. Remediation techniques based on CO_3/HCO_3 extraction of uranium may also result in calcite precipitation. Mason et al. (1997), for example, found leachate supersaturated with respect to calcite after a simulated heap-leach experiment involving uranium-contaminated soil and observed calcite precipitation. Uptake of uranyl by precipitating calcium carbonate may influence the efficacy of such remediation strategies.

The incorporation of uranium in calcite and aragonite also provides the basis for U-series age-dating methods, which have proven to be valuable geochronological tools for studies of both marine and terrestrial carbonates. The uranium incorporated into marine calcite and aragonite has also been used as a record of its past concentration in seawater (Russell et al., 1994) and to examine climatic variations over time (Shen and Dunbar, 1995; Min et al., 1995). Uranium is usually enriched in arago-

* Author to whom correspondence should be addressed (rjreeder@notes.cc.sunysb.edu).

nitic marine organisms relative to calcitic ones (e.g., Broecker, 1963), and experimentally determined partition coefficients confirm that U(VI) is preferentially incorporated into aragonite relative to calcite (Kitano and Oomori, 1971; Meece and Benninger, 1993).

The question of U(VI) binding mechanisms is fundamental for understanding both its uptake behavior and the potential for loss, or remobilization. If the uranyl substitutes in the calcite structure, resulting in a dilute solid solution (cf. Swart and Hubbard, 1982), remobilization may require bulk dissolution. However, the solubility of a uranyl-containing calcite may be significantly greater than that of pure calcite. On the other hand, if uptake results in formation of a discrete uranium-rich phase (not calcite), then remobilization may be controlled by the solubility of this second phase. Consequently, knowledge of the solid speciation of uranium taken up by calcite is essential for understanding sequestration and for predicting its long-term retention. The presence of uranium in natural calcite, including in geologically old samples, clearly demonstrates the possibility of long-term stability. In most natural samples, however, the speciation (including oxidation state) is rarely known. Uranium concentrations in calcite are typically less than 10 ppm. Such low concentrations, however, may simply reflect low uranium concentrations in the natural fluids from which they formed, rather than remobilization.

In a previous study we examined differences in local coordination of uranyl species coprecipitated with calcite and aragonite (Reeder et al., 2000). These coprecipitation experiments were conducted at pH 8.1 to 8.2, with the dominant aqueous uranyl species being the triscarbonato complex, $UO_2(CO_3)_3^{4-}$. This species is characterized by bidentate coordination of the three CO_3 groups in the equatorial plane of the UO_2 moiety (cf. Clark et al., 1995). X-ray absorption fine structure (XAFS) spectroscopy and luminescence spectroscopy revealed that essentially the identical structural unit was present in the uranyl-containing aragonite, suggesting that the aqueous species was incorporated virtually intact, i.e., without any disruption of the equatorial coordination. In contrast, a different equatorial coordination was identified for the uranyl-containing calcite; the equatorial oxygen shell was closer to the uranium and with apparently fewer oxygen atoms. This indicated that a change in the equatorial coordination was required for incorporation into calcite, in contrast to the case for aragonite. The XAFS results also failed to reveal the configuration of more distant oxygens of the CO_3 groups and no Ca atoms from the host calcite were identified (unlike the results for aragonite). These findings suggested that the local coordination of the uranyl species incorporated into the calcite was disordered, reflecting multiple environments. Indeed, the results of time-resolved luminescence spectroscopy indicated the presence of multiple uranyl species in the uranyl-containing calcite. It was suggested that the apparent disorder probably reflects steric limitations in accommodating the uranyl species in the calcite structure, and further speculated that the disorder in calcite indicated a less stable local coordination for U(VI) in calcite than in aragonite.

Important questions remain regarding uptake of U(VI) by calcite. One issue is whether differences in solution chemistry and pH would influence the coordination of the uranyl incorporated in the calcite. That can be addressed by changing solution chemistry; however, requirements to maintain adequate supersaturation place restrictions on the range of variations that are practical. Another issue relates to a possible cause for multiple uranyl species in the calcite. Other coprecipitation studies at the calcite $(10\bar{1}4)$ face, its most common growth surface, have demonstrated that incorporation of divalent metals occurs at structurally distinct surface sites resulting in different uptake preferences (Paquette and Reeder, 1995; Reeder, 1996). It is important to know if differential uptake at structurally distinct surface sites occurs and whether that may be a possible cause for the multiple species observed in the calcite. In the present study we report new XAFS and luminescence results from uranyl-doped calcite that begin to address these questions. Our results reveal that surface controls are significant, resulting in heterogeneous uptake on calcite surfaces. We also provide new insight to the nature of the local coordination of uranyl in synthetic calcite.

2. EXPERIMENTAL METHODS

2.1. Coprecipitation Procedures

Two different growth techniques were used for uranyl coprecipitation with calcite. Method I followed the procedure described by Reeder et al. (2000) and is similar to the method used by Tesoriero and Pankow (1996). $CaCl_2$ and $NaHCO_3$ solutions were delivered at a constant rate using a dual syringe pump to a stirred reaction vessel through which air was bubbled continuously. Solution Ca and HCO_3 concentrations were maintained at approximately 10 mM. NaCl was used as a background electrolyte to give an ionic strength of 0.5 molal. The pH initially increased until calcite nucleation was observed, then dropped to 8.1 to 8.2 and remained constant throughout the duration of the coprecipitation experiment. Aqueous uranyl nitrate solution (50 μM final solution concentration) was added after the pH stabilized, and the $CaCl_2$ syringe was exchanged for one that contained $CaCl_2$ with a predetermined amount of uranyl nitrate to account for the small amount taken up by calcite during growth. A high-purity $CaCl_2$ reagent was used to minimize contamination of the calcite with Sr, which has a fluorescence emission slightly overlapping the $L\alpha_1$ line for uranium. This allowed us to use fluorescence detection methods for X-ray absorption fine structure (XAFS) spectroscopy at the U L_3-edge. The calculated saturation index was in the range SI = 1.4 to 1.5. Solutions were undersaturated with respect to rutherfordine (UO_2CO_3) and schoepite ($UO_3{\cdot}2H_2O$), which are potentially limiting for uranyl solubility. The finely crystalline calcite product was recovered by vacuum filtration, washed multiple times in deionized water, and dried at 50°C. Scanning electron microscope images reveal that the crystallites dominantly exhibit the common rhombohedral morphology. X-ray diffraction failed to reveal any lines other than those for calcite. The uranium concentration in this calcite is approximately 725 ppm. This U concentration and the U/Ca ratio of 0.005 in the growth solution give an average empirical partition coefficient of 0.06, which is consistent with values reported by Kitano and Oomori (1971) and Meece and Benninger (1993).

A second procedure (method II) was used for coprecipitation at a slightly lower pH and to obtain single crystals of calcite that would allow study of site-selective uptake on the surface. Method II is a modified free-drift method described in detail by Paquette and Reeder (1995) and Reeder (1996). Growth occurs in a sealed reaction vessel with headspace in contact with a reservoir of solid ammonium carbonate. Steady-state decomposition of the ammonium carbonate produces $NH_3(g)$ and $CO_2(g)$, which dissolve into the $CaCl_2$-NH_4Cl growth solution simultaneously increasing pH and carbonate alkalinity. Solution pH initially increases until calcite crystals begin nucleating on immersed glass substrates and vessel walls. The pH remains nearly constant (7.5–7.6) for as long as one week as calcite crystals increase in size, driven by the near steady-state supply of carbonate. Aqueous uranyl nitrate was added after solution pH stabilized (following nucleation). Despite the nearly constant pH during the coprecipitation period, the initial Ca^{2+} concentration (10 mM) decreased over the duration of the experiment (by up to 40%), and hence the solution composition was not strictly constant. Initial U concentrations were 4

and 40 μM for different experiments, and decreased by less than 20% over the duration of growth. Total CO_2 was determined in parallel experiments using the procedure described by Hall and Aller (1992). This coprecipitation method requires a high ionic strength ($\sim$1.75 mol/L), using NH_4Cl as a background electrolyte. Calculated saturation indexes were in the range 0.6 to 0.8. Water-clear calcite single crystals up to 700 μm were recovered from substrates, washed repeatedly in deionized water, and dried in air at 50°C. Examination of the crystals showed them to be nearly perfect rhombohedra, exhibiting the common growth form {10$\bar{1}$4}. The growth surfaces appear macroscopically flat under reflected light, but differential interference contrast (DIC) microscopy reveals polygonized growth spirals. Hence, growth occurred by the spiral mechanism, wherein attachment occurs primarily at kink sites within steps, which sweep around a dislocation growth center. Based on previous experiments using this technique, we anticipated that this growth condition would reveal whether surface structural factors control uptake of uranyl. Final uranium concentrations were determined by spatially resolved X-ray fluorescence (see below), yielding average concentrations of $\sim$15 and $\sim$225 ppm for the lower and higher solution uranium concentrations, respectively. Portions of the single crystals were ground to a fine powder for bulk XAFS and luminescence spectroscopy. Other single crystals were selected for micro-XAS work.

2.2. X-ray Absorption Fine Structure Spectroscopy (XAFS)

XAFS spectra were collected on powdered samples and on aqueous standards at beamline X11A of the National Synchrotron Light Source (NSLS) at Brookhaven National Laboratory. The storage ring was operated at 2.5 GeV with a maximum current of 290 mA. Multiple scans were taken for each sample over the U L_3-edge (17166 eV) using a pair of Si(111) monochromator crystals, with one crystal detuned by $\sim$30% for harmonic rejection. Solid samples were mounted in cavities in aluminum holders covered with Kapton tape and secured in a cold-finger positioned at 45° to the X-ray beam. Samples were held near 77 K using a liquid nitrogen cryostat, which improved the signal/noise ratio. Absorption spectra for uranyl-doped calcite samples were obtained using fluorescence detection with a 13-element solid-state Ge detector. Spectra for aqueous standards were obtained using a Stern-Heald type detector. Spectra of uranyl-containing model compounds were obtained in a previous study (Reeder et al., 2000) using transmission methods. Based on calibration of the edge position relative to a yttrium metal foil, the first inflection point of the uranyl-containing spectra was assigned a value of 17171 eV. All spectra were calibrated before summing.

Data analysis included subtraction of a linear preedge background, normalization, and conversion to k-space, followed by μ_0 fitting using a cubic spline. The $\chi(k)$ function was Fourier transformed using k^2 weighting, and all fitting was done in R-space using WinXAS (Ressler, 1997) and theoretical backscattering amplitudes and phase shifts calculated using FEFF7 (Zabinsky et al., 1995). Several starting models were used for the FEFF7 calculations, including the mineral liebigite [$Ca_2UO_2(CO_3)_3{\cdot}11H_2O$] and idealized clusters of a uranyl triscarbonato complex (three bidentate CO_3 groups) and a similar cluster with one monodentate and two bidentate CO_3 groups. No significant differences in final fit results were observed using paths from these various starting models. A single threshold energy value (ΔE_0) was allowed to vary during fitting. The amplitude reduction factor, S_0^2, was fixed at a value of one based on fitting of model compounds. Errors in the fit parameters, estimated from fits of well-characterized model compounds, are $\pm$ 20% for coordination number (CN), $\pm$ 0.02 Å for first and second shell distances (R), and $\pm$ 0.03 Å for greater distances. Debye-Waller type factors (σ^2) have approximate error of $\pm$ 0.002 Å^2.

2.3. Micro Synchrotron X-ray Fluorescence (μ-XRF) and X-ray Absorption Near-edge Structure Spectroscopy (μ-XANES)

Uranyl-containing calcite single crystals exhibiting a single growth spiral on a (10$\bar{1}$4) growth surface were sectioned and polished to produce a $\sim$30 μm thick slice retaining the as-grown surface, and mounted on ultra-high-purity glass disks (cf. Reeder, 1996). The uranium distribution was mapped initially using the μ-XRF beamline X26A (National Synchrotron Light Source, Brookhaven National Laboratory). For this work, Kirkpatrick-Baez (K-B) type mirrors were used to focus a monochromatic X-ray beam ($\sim$17500 eV) to a 15 $\times$ 15 μm spot on the sample, which was positioned at 45° to the X-ray beam. Characteristic fluorescence was detected using a solid-state Si(Li) detector positioned at 90° to the beam direction. Concentrations were determined by standardless analysis, with instrumental parameters determined using an anorthite glass standard and a trace element-containing calcite standard (Reeder, 1996). Precision is estimated to be $\pm$5% relative, with minimum detection limits of approximately 1 to 2 ppm for uranium.

Subsequent μ-XRF elemental maps and polarized μ-XANES spectra (U L_3-edge; 17166 eV) were obtained at the undulator beamline 20-ID-B at the Advanced Photon Source (Argonne National Laboratory). Si(111) monochromator crystals were used to create a monochromatic beam, which was focused using K-B mirrors to form a 5 $\times$ 6 μm spot on the sample. The entrance slits to the K-B mirrors were set at 0.3 $\times$ 0.3 mm, 50 m from the source. This gave an energy resolution of approximately $\Delta E/E = 1.3 \times 10^{-4}$, or 2.2 eV. The calcite crystal section was mounted at either 45° or 60° to the incident X-ray beam and was rotated in one of those planes to achieve a desired orientation between the single crystal and the incident X-ray beam. A 13-element solid-state Ge detector positioned at 90° to the beam was used to collect characteristic fluorescence; for μ-XRF mapping the energy was set at $\sim$15 eV above the U L_3-edge.

2.4. Luminescence Spectroscopy

Time-resolved luminescence spectra were collected using a SPEX Industries Fluorolog 2 system with a Model 1934D phosphorimeter attachment for the flashlamp excitation source (400–420 nm) as described elsewhere (Clark et al., 1999). The detection window was gated from 0.04 to 2.0 ms unless otherwise stated. The afterglow from the flashlamp extends to $\sim$0.05 ms precluding the collection of time-resolved data at times shorter than this.

3. RESULTS

3.1. Aqueous Speciation

The distribution of aqueous species in the method I growth solution was calculated with the program PHREEQC (Parkhurst, 1995) using the database from MINTEQA2 (Allison et al., 1991). Data for aqueous uranyl species were supplemented with those from the Nuclear Energy Agency thermochemical database (Grenthe et al., 1992), or their stability constants were adjusted to be consistent with NEA values. We also included the aqueous uranyl complex $Ca_2UO_2(CO_3)_3$(aq) reported by Bernhard et al. (1996). The Davies equation was used for calculation of activity coefficients of charged uranyl species. The method I growth solution was similar to that used in our earlier coprecipitation study (Reeder et al., 2000). The calculated speciation diagram (Fig. 1a) shows that >95% of the uranium is present as the uranyl triscarbonato complex, $UO_2(CO_3)_3^{4-}$ (aq), at pH 8.2.

Aqueous speciation calculations for the method II solution were limited by the lack of data appropriate for modeling the high ionic strength U(VI)-Ca-NH_4-HCO_3-Cl solutions ($\sim$1.75 mol/L). At such ionic strength the Davies equation is not expected to yield reliable activity coefficients for the charged uranyl complexes, resulting in significant uncertainty in predicted speciation. Use of Pitzer equations provides more accurate speciation models at high ionic strengths, however, the necessary interaction parameters for uranyl species have not yet been determined (Felmy and Rai, 1999). Plyasunov et al. (1998) suggested a method for estimating Pitzer equation parameters for uranyl-containing solutions. Pitzer interaction parameters for uranyl species estimated using this approach have

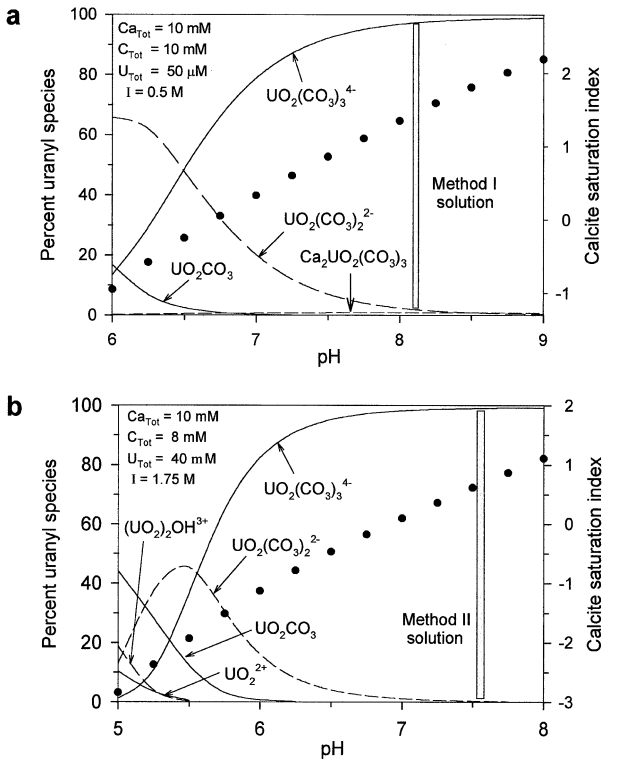

Fig. 1. Calculated aqueous U(VI) speciation in growth solutions as a function of pH for uranyl coprecipitation with calcite: (a) method I (pH ~8.2) and (b) method II (pH ~7.6). Calculated calcite saturation index is shown by the heavy dotted line. Only the most abundant species are shown. See text for further details.

been incorporated into the program GMIN (Felmy, 1995; pers. comm.). Because no interaction parameters were available for NH_4-Cl, we modeled the solutions using Na-Cl parameters. Additional uncertainty in the predicted speciation is associated with a gradual depletion of Ca over the duration of the coprecipitation. The estimated distribution of uranyl species in the method II solution is shown in Figure 1b. In the pH range of interest, >98% of the uranium is present as the uranyl triscarbonato complex, as in the method I solution. Although these results should be considered no more than a best estimation, it seems likely that the uranyl triscarbonato species dominates both the method I and method II solutions.

3.2. Luminescence Spectroscopy

The luminescence spectrum for the uranyl incorporated during method I calcite growth (Fig. 2) is nearly identical to that for the uranyl-doped calcite studied previously (Reeder et al., 2000), which was grown using the same technique and with similar solution chemistry. This spectrum is red-shifted by ~15 nm relative to that for uranyl-containing aragonite (Fig. 2). The luminescence spectrum for the higher concentration method II uranyl-containing calcite shows subtle differences and is very slightly blue-shifted relative to the method I calcite (Fig. 2), yet it is also distinct from the uranyl-containing aragonite. Single exponential decays yielded luminescence lifetimes $\tau = 150$ μs for the method I calcite and $\tau = 190$ μs for the method II

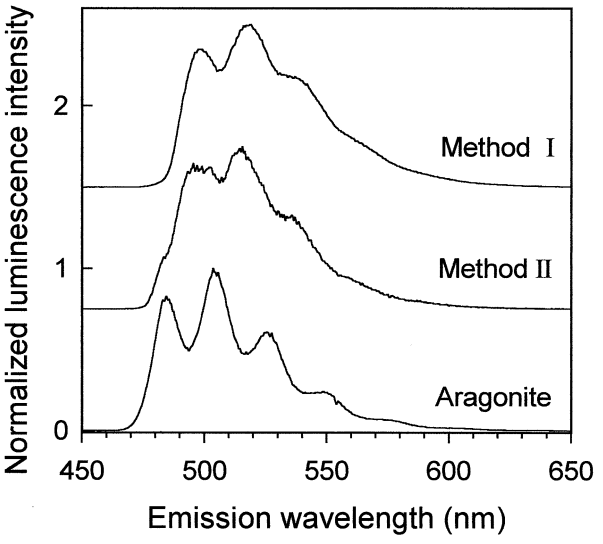

Fig. 2. Low-temperature (~77 K) luminescence spectra of method I and II uranyl-doped calcites and uranyl-doped aragonite.

calcite. However, a closer inspection of the single exponential fit for the method II calcite (Fig. 3) indicates significant deviations from the data, suggesting the presence of more than one significant luminescing species.

To test for multiple species, spectra were collected in which the gate for collecting emitted photons was only open for a short time period after excitation (0.05–0.20 ms) and then additionally gated for collecting photons at longer delay times (0.40–1.5 ms). These two spectra (Fig. 4) emphasize the shorter-lived component(s) and longer-lived component(s), respectively. The two gated spectra from the method II calcite are indeed distinct from one another. The short-gated spectrum exhibits a very close similarity to the spectrum for the method I calcite, suggesting that the shorter-lived species in the method

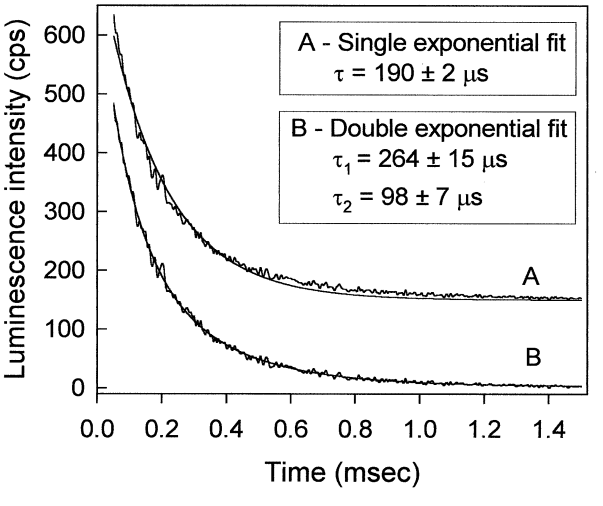

Fig. 3. Low-temperature (~77 K) decay kinetics for uranyl-doped calcite prepared by method II. Curves labeled A and B show the fits using one and two exponents, respectively. The excitation source was at 400 nm, and the decay was monitored at 514 nm.

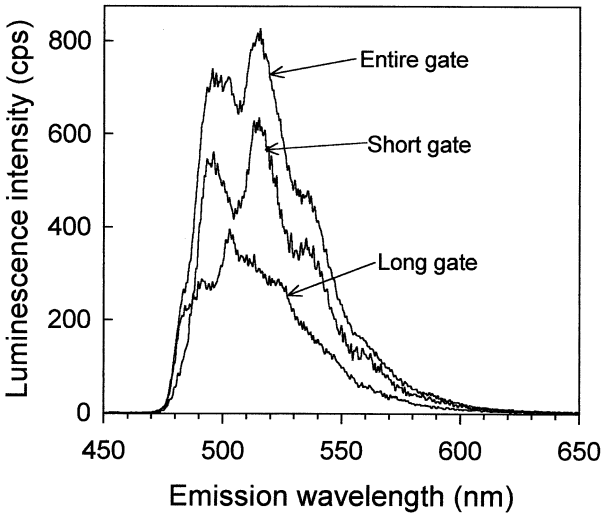

Fig. 4. Low-temperature (~77 K) gated luminescence spectra for uranyl-doped calcite prepared by method II. The peak heights of the spectra have been adjusted for easier comparison; the raw data for the long-gated spectrum is only about 1/3 as large as the spectrum from the total gate. See text for further description.

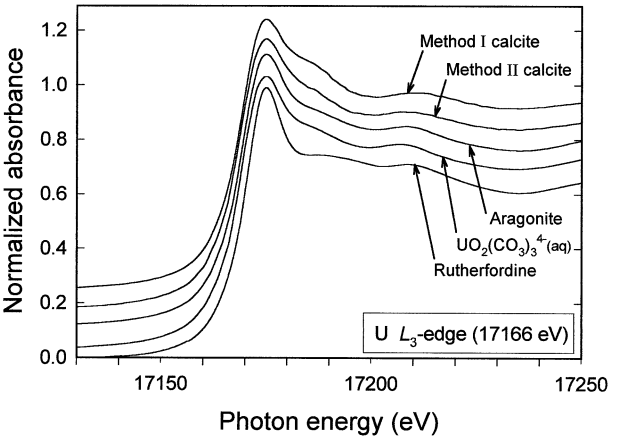

Fig. 6. Near-edge regions of the uranium L_3-edge absorption spectra for uranyl-containing calcites, compared with spectra for uranyl-containing aragonite, an aqueous uranyl triscarbonato standard, and rutherfordine (UO_2CO_3). Differences are observed in the shoulder (centered 10–15 eV above the absorption maximum), which has been attributed to multiple scattering within the uranyl moiety. Rutherfordine spectrum is from the study of Thompson et al., 1997.

II sample is similar to that observed in the method I sample. The spectrum obtained with the longer-gate delay clearly contains contributions from the shorter-lived emissive species. However, these two spectra can be mathematically manipulated to obtain a better spectral representation of only the longer-lived species. Specifically, if the short-gate spectrum is reduced by a scaling factor of 56% (to account for the contribution of the short-lived species to the longer-gate delay spectrum) and subtracted from the longer-gated spectrum, a difference spectrum is obtained (shown in Fig. 5). The scaling factor was determined empirically based on the optimum resolution of the vibronic bands in the difference spectrum. This difference spectrum is very similar to that reported previously for uranyl in aragonite, indicating that the longer-lived species in the method II sample is similar to that in aragonite.

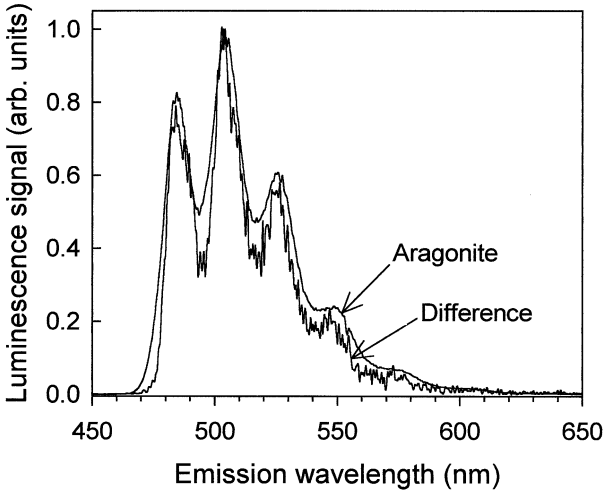

Fig. 5. Comparison of uranyl luminescence spectra from aragonite and that generated from subtracting the short-gated spectrum from the raw long-gated spectrum of the method II calcite (see text). This latter spectrum therefore represents the unique species that becomes apparent in the long-gated spectrum of the method II calcite.

The aqueous biscarbonato uranyl species does not luminesce owing to quenching under solution conditions (Kato et al., 1994; Meinrath, 1998) so that a comparison with either gated spectrum in Figure 4 was not possible. Significantly improved fits of the luminescence decay data for the method II sample were obtained using a two-exponent decay function (Fig. 3), yielding lifetimes of 98 μs and 264 μs. The latter of these is also consistent with the lifetime obtained at ~77 K for uranyl incorporated into aragonite.

Comparison of the short- and long-delay gated spectra for the uranyl-containing calcite prepared by method I shows that they are only subtly different from one another. This suggests that similar species dominate the method I calcite as described previously (Reeder et al., 2000) and here, as well as being present in the method II calcite.

3.3. XANES and EXAFS of Bulk Samples

Near-edge regions of the X-ray absorption spectra for the uranyl-containing calcites are shown in Figure 6, along with spectra for a uranyl triscarbonato aqueous reference sample, the uranyl-containing aragonite studied previously, and rutherfordine (UO_2CO_3). The most notable differences are evident in the shoulder centered at 10 to 15 eV above the absorption maximum. Hudson et al. (1995) attributed this shoulder to the multiple-scattering resonance within the linear O=U=O moiety. The shoulder is more pronounced in the spectrum of the method I calcite compared to the aqueous triscarbonato species or the aragonite, which are very similar. In the method II calcite the shoulder appears to be intermediate between those for the method I calcite and aragonite. The shoulder is significantly

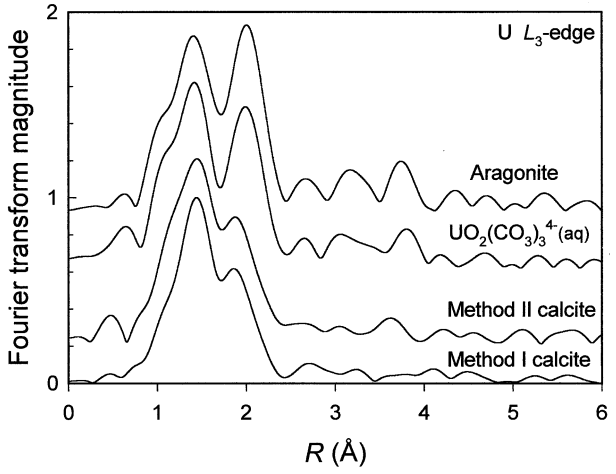

Fig. 7. Fourier transform magnitudes (not corrected for phase shifts) of the two uranyl-containing calcites (bottom) compared with a uranyl-doped aragonite studied previously and an aqueous triscarbonato standard.

diminished in the rutherfordine spectrum (30 K), which is taken from the study of Thompson et al. (1997).

The Fourier transform magnitudes for both uranyl-containing calcites show the distinct low-R peak characteristic of the two axial oxygen atoms (O_{ax}) with a smaller, partly overlapping peak associated with the equatorial coordination shell (Fig. 7). These FT magnitudes differ from those for uranyl-doped aragonite (Reeder et al., 2000) and aqueous uranyl triscarbonato species, both of which show the peak for the equatorial shell well separated from the peak for the axial oxygens. Because coprecipitation method I was similar to that used in our previous study (Reeder et al., 2000), we expected similar XAFS fit results, and this was largely the case. Because of the potential for multiple uranyl species in the calcite, several approaches were tried in fitting, using different combinations of shells to model the equatorial coordination. Initial fits were constrained to having a shell with two axial oxygens, a shell for nearest equatorial oxygens, a shell for carbon atoms, and a multiple-scattering (MS) path at twice the U-O_{ax} distance. A best fit yielded 2 axial oxygens at 1.80 Å, 5.6 equatorial oxygens at 2.33 Å, and 3.1 carbons at 2.90 Å (Table 1). A representation in k-space of the best fit is labeled A in Figure 8. A multiple scattering path (O_{ax1}-U-O_{ax2}-U) was found to be important in all fits at twice the U-O_{ax} distance (or ~3.6 Å).

The quality of the overall fit is only fair visually, suggesting that a single equatorial oxygen shell may be inadequate. Efforts to improve the fit relied on splitting the equatorial oxygen coordination into two shells and allowing for a second carbon shell. Physically this would represent different types of coordination of the CO_3 groups in the equatorial plane (e.g., monodentate and bidentate). The number of parameters allowed to vary during a fit was always less than that allowed by the Nyquist limit based on the k and R ranges. A best fit using split shells is labeled B in Figure 8. The first O_{eq} shell has 3 to 4 oxygens at 2.29 Å; the second shell has 2 to 3 oxygens at 2.40 Å. Carbon shells are at 2.85 and 2.99 Å. This resulted in slight visual improvements in the overall fit, but we emphasize that any improvement may not be statistically significant. Moreover, the separations of these split shells are 0.11 and 0.14 Å, respectively. Because of the range in k-space used (~11.5

Table 1. Uranium L_3-edge XAFS Fit Parameters for Uranyl-containing Calcite Samples.

Method I calcite (single equatorial shell)			
Shell	CN[a]	R (Å)[b]	σ^2 (Å^2)[c]
U-O_{ax}	2[d]	1.80	0.002
U-O_{eq}	5.6	2.33	0.009
U-C	3.1	2.90	0.007
MS[e]	2.4	3.60	0.005
ΔE_0[f]	4.9		

Method II calcite[g] (single equatorial shell)			
Shell	CN	R (Å)	σ^2 (Å^2)
U-O_{ax}	2	1.80	0.004
U-O_{eq}	5.7	2.36	0.009
U-C	3.2	2.92	0.004
MS[e]	2.7	3.60	0.006
ΔE_0	5.4		

Method I calcite (split equatorial shells)			
Shell	CN	R (Å)	σ^2 (Å^2)
U-O_{ax}	2	1.79	0.003
U-O_{eq1}	3.6	2.29	0.009
U-O_{eq2}	2.7	2.40	0.006
U-C_1	2.1	2.85	0.003
U-C_2	1.1	2.99	0.003
MS[e]	2.6	3.59	0.006
ΔE_0	4.9		

Method II calcite (split equatorial shells)			
Shell	CN	R (Å)	σ^2 (Å^2)
U-O_{ax}	2	1.80	0.003
U-O_{eq1}	2.3	2.28	0.003
U-O_{eq2}	3.9	2.43	0.003
U-C_1	3.1	2.92	0.005
U-C_2	—[h]	—	—
MS[e]	2.7	3.60	0.004
ΔE_0	5.5		

[a] Coordination numbers have errors of ± 20%.
[b] Errors on distance are ± 0.02 Å.
[c] Errors on Debye-Waller type disorder parameters are ± 0.002 Å^2.
[d] Fixed at 2 for most fits, but refined to a value near 2 for test fits.
[e] Four-legged multiple scattering path O_{ax1}-U-O_{ax2}-U.
[f] Global energy threshold varied during fitting.
[g] For the method II calcite, additional weak peaks fitted: ~1 oxygen at 4.15 Å (σ^2 fixed at 0.005) and CN ~2 for multiple-scattering path (O_{dist}-C-U) at 4.18 Å (σ^2 fixed at 0.008).
[h] Not fitted.
k-range: 3.00–14.20 Å^{-1} (method I); 2.98–13.62 Å^{-1} (method II).
R-range: 0.59–3.50 Å (method I); 0.69–4.10 Å (method II).

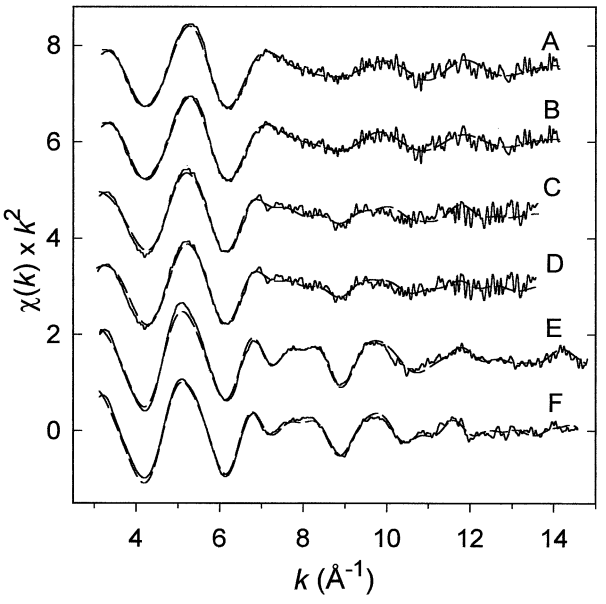

Fig. 8. Experimental k^2-weighted chi(k) curves (solid) and fits (dashed) for the uranyl-containing carbonate samples. (A) Method I calcite using a single equatorial oxygen shell for fitting. (B) Method I calcite using two separate equatorial oxygen shells. (C) Method II calcite using a single equatorial oxygen shell. (D) Method II calcite using two separate equatorial oxygen shells. (E) Aragonite from Reeder et al. (2000). (F) Aqueous uranyl triscarbonato species, $UO_2(CO_3)_3^{4-}$, at pH 9.7. See text for further details.

$Å^{-1}$), shells closer than ~0.14 Å cannot be resolved with much certainty. In contrast, Sylwester et al. (2000) readily identified splitting of the equatorial oxygen shell for inner-sphere uranyl surface complexes on silica, alumina, and montmorillonite. In that case, the separation of the shells was 0.18 to 0.19 Å, and distinct peaks were evident in the FT magnitudes. Therefore, any splitting of the equatorial shell in our samples is expected to be less and may not be resolved.

The absence of significant features in the FT magnitude at distances beyond the carbon atoms is noteworthy and suggests that more distant backscatterers (e.g., O_{distal}, Ca, etc.) do not lie in a uniform path. Reeder et al. (2000) interpreted this to indicate a largely disordered environment beyond the nearest equatorial shells. The absence of U-U backscattering makes clustering or the presence of polymeric uranium species unlikely.

Fitting for the method II calcite yielded generally similar fit parameters, but with slightly longer equatorial distances (Table 1). Best fit results gave 2 axial oxygens at 1.80 Å, 5.7 oxygens at 2.36 Å, and 3.2 carbons at 2.92 Å (C in Fig. 8). Using a split equatorial oxygen shell yielded distances at 2.28 and 2.43 Å (Table 1), but resulted in only slight improvements in overall fit (D in Fig. 8). Weak features at higher R could be fitted with minor contributions from a distal oxygen and a multiple scattering path at 4.15 and 4.18 Å, respectively.

Because XAFS averages over the backscattering contributions for all absorbers, there are clearly limitations to the information provided by these results. If multiple local environments exist around the uranium atoms, their contributions are superimposed in the $\chi(k)$ curves. In cases where the identities of all the multiple species are known [and model $\chi(k)$ curves are known], it may be possible to use least-squares methods to fit linear combinations of model curves to estimate the relative contributions of the different species. The luminescence results indicate that one species present in the method II calcite is the same as found in aragonite. However, we do not know the identity of the other species, which also dominates the method I calcite. Principal component analysis has also been used with some success to aid in identifying different species, but this approach requires a series of spectra containing the components of interest.

3.4. μ-XRF and μ-XANES of Single Crystal ($10\bar{1}4$) Calcite Growth Surfaces

The calcite single crystals obtained from coprecipitation method II consistently exhibited ($10\bar{1}4$) growth faces. Differential interference contrast (DIC) microscopy showed these growth faces to be composed of polygonized growth spirals (i.e., hillocks) indicating that growth occurred by the spiral (i.e., Burton-Cabrera-Frank layer) mechanism. Figures 9a and 9c show DIC images of as-grown ($10\bar{1}4$) surfaces of uranyl-doped calcite crystals. The faces contain a single polygonized growth hillock composed of four vicinal faces. Each vicinal face appears as a uniform polygon, but at a nanometer scale is composed of an array of parallel (dominantly monolayer) growth steps separating terrace sections. The four vicinal faces differ by the orientation of the growth steps composing them and the direction of their advance during growth. Because of the c-glide symmetry element perpendicular to the face (Fig. 9e), steps labeled $[\bar{4}41]_+$ and $[48\bar{1}]_+$ are symmetrically equivalent, and steps $[441]_-$ and $[48\bar{1}]_-$ are symmetrically equivalent; but + steps are not equivalent to the − steps. The geometry and surface/bulk symmetry relationships of these growth hillocks have been described in detail (Staudt et al., 1994; Paquette and Reeder, 1995; Reeder, 1996; Reeder and Rakovan, 1999), and their growth activity has been observed in situ using atomic force microscopy (Gratz et al., 1993; Teng et al., 1998). The presence of these hillocks is significant because uranyl species can become incorporated into structurally distinct steps of the nonequivalent vicinal faces during growth. Previous coprecipitation studies have demonstrated that divalent metals (e.g., Mn, Co, Zn, Sr, Ba, and Cd) are incorporated differentially between the nonequivalent vicinals, by as much as a factor of ten difference in concentration (cf. Reeder and Rakovan, 1999), reflecting that the different incorporation sites have distinct preferences for metal uptake during layer growth. Moreover, different metals exhibit different step preferences, depending in part on ion size and coordination preferences. The spatial segregation of the different sites and steps into well defined regions on the crystal face by the activity of the growth spiral makes it possible to compare their relative uptake preferences by examining concentration differences in the regions of the crystal under each vicinal face.

We examined the ($10\bar{1}4$) surfaces of several uranyl-doped calcite crystals using the micro-beam capabilities at the μ-XAS beamlines X26A at the NSLS and 20-ID-B at the APS. There is a striking difference in the distribution of uranium corresponding precisely to the nonequivalent vicinal faces on the surface (Fig. 9b and 9d). The portions of the crystal represented

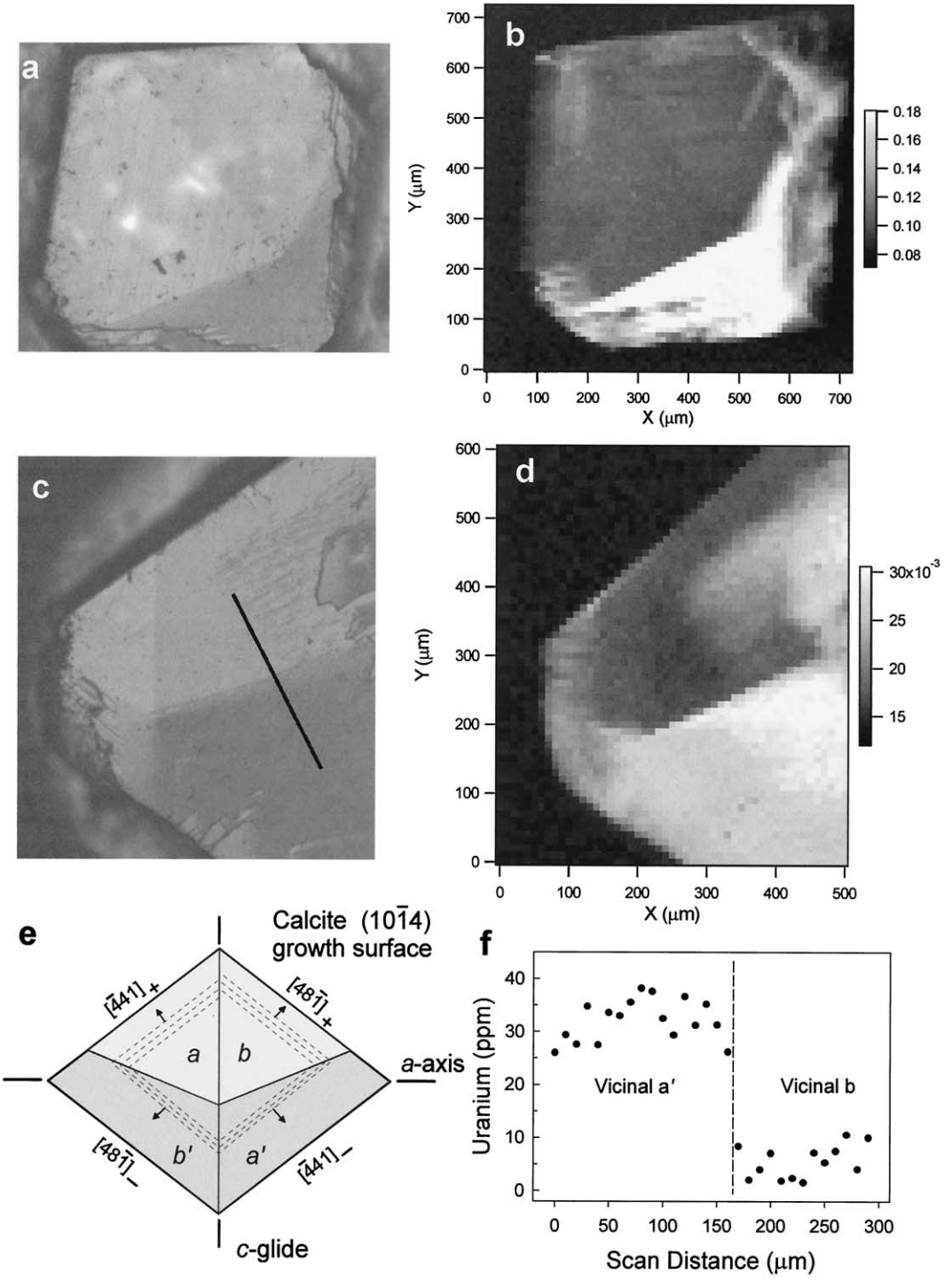

Fig. 9. (a–d) Differential-interference contrast (DIC) images (left) and corresponding μ-XRF maps showing uranium distribution (right) for as-grown (10$\bar{1}$4) surfaces of two uranyl-doped (method II) calcite crystals (lower total uranium concentration). The different shading patterns in DIC images (a and c) correspond to nonequivalent vicinal faces, which compose the flanks of polygonized growth hillocks resulting from spiral growth. In μ-XRF maps (b and d) the lighter shading corresponds to higher uranium concentrations. (e) Schematic diagram showing the geometry of a single polygonized growth hillock on a calcite (10$\bar{1}$4) surface. The dashed lines indicate the orientations of growth steps, which differ in adjacent vicinal faces. Small arrows show directions of translation of growth steps in each vicinal face. The *c*-glide symmetry element, which is normal to the face, symmetrically relates vicinals a and b (lighter shading) and also vicinals a' and b' (darker shading). However, vicinals a and a' (and b and b') are symmetrically nonequivalent. The a' and b' vicinals are systematically enriched in uranium relative to the a and b vicinals. (f) Uranium concentration along the transect line in DIC image (c) showing the sharp contrast in uranium incorporation between nonequivalent vicinal faces.

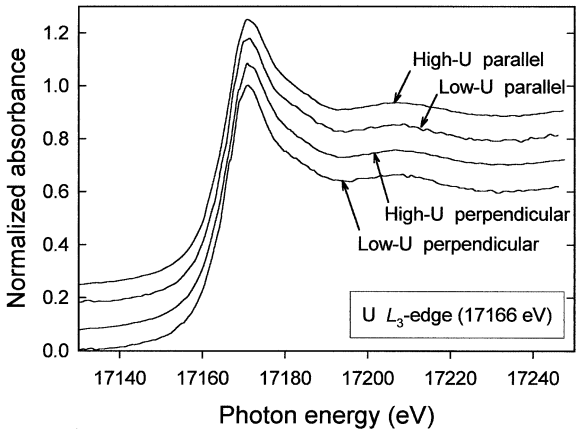

Fig. 10. Polarized U L_3-edge XANES spectra taken from adjacent, nonequivalent vicinal faces (indicated as high U or low U) on a method II calcite single crystal. XANES spectra are compared for orientations of the polarization vector parallel and perpendicular to the crystallographic *c*-axis.

by vicinals designated a' and b' (see Fig. 9e) are strongly enriched in uranium relative to portions under vicinals a and b. No apparent concentration difference is observed between symmetrically equivalent vicinals (e.g., a and b). In the calcite crystals grown with lower total uranium, the concentration in the regions associated with the a and b vicinals averages approximately 4 to 5 ppm U, whereas the concentration in the adjacent a' and b' vicinals averages 30 ppm U (Fig. 9f). In the crystals grown in solutions with higher total uranium concentrations, the a and b vicinals are typically in the 40 to 50 ppm range, whereas the concentration in the adjacent a' and b' vicinals is 400 to 500 ppm U. Thus, the magnitude of differential uptake is approximately a factor of 6 to 10. This anisotropy indicates that uranyl is dominantly incorporated at the surface sites that occur on the a' and b' vicinals. Consequently, the presence and availability of these sites (and the growth steps in which they occur) on calcite surfaces are significant controls on the uptake potential of (at least some) uranyl species.

The finding that uranium uptake occurs at distinct surface sites on the calcite (albeit in significantly different proportions) posed the interesting prospect of accounting for the multiple uranyl species observed by luminescence spectroscopy. To test this we collected U L_3-edge XANES spectra of the different regions of the uranyl-containing calcite grown from the nonequivalent vicinal faces. This was carried out at the undulator beamline 20-ID-B (APS) using a monochromatic beam focused to approximately 5×6 μm and positioned in adjacent nonequivalent vicinal faces using a microscope. Because of the strong linear polarization of the X-ray beam in the horizontal plane, we collected XANES spectra with the crystal in several orientations with respect to the polarization vector, e.g., parallel and perpendicular to the *c*-axis of the calcite. The μ-XANES spectra are shown in Figure 10. No discernible difference can be seen between the spectra in adjacent nonequivalent vicinals for any particular orientation of the crystal relative to the polarization vector. Similarly, no orientation dependence is evident for spectra in any given vicinal face.

4. DISCUSSION

Several lines of evidence indicate that the uranyl is primarily incorporated into the calcite structure and not present in a second phase. Speciation calculations showed that the growth solutions were undersaturated with respect to likely solubility-limiting uranyl phases, including rutherfordine (UO_2CO_3) and schoepite ($UO_3 \cdot 2H_2O$). Liebigite [$Ca_2UO_2(CO_3)_3 \cdot 11H_2O$] is also an unlikely precipitate in view of its reported solubility (Amayri et al., 1999). XRD scans of the samples using low-background sample holders failed to show any indication of a second phase, and all calcite lines were identified. The XANES spectra of the uranyl-containing calcites differ from those of rutherfordine and samples containing only uranyl triscarbonato clusters. The FT magnitudes and XAFS fit results show no indication of U-U backscattering, which would be expected for a uranyl-rich phase. Further, there is no evidence for the distinctive luminescence pattern of schoepite in the emission spectra of either sample. The luminescence lifetime of the minor triscarbonato component in the method II calcite is significantly longer than that reported for the luminescing calcium triscarbonato aqueous species (Bernhard et al., 1996), suggesting that fluid inclusions are not a source of the detected uranyl. Finally, the observation that the uranium distribution in the method II single crystals correlates exactly with the distribution of nonequivalent growth steps (consistent with the surface symmetry of the host calcite) strongly suggests that the detectable uranium is incorporated in the calcite structure. Although it may never be possible to entirely rule out the presence of a second phase, our observations indicate that no detectable amount of uranium is present in such form.

4.1. Local Coordination of UO_2^{2+} in Calcite

Our present observations from XAFS and luminescence spectroscopy of the different calcite samples show that aqueous solution and growth conditions have an influence on the local coordination of uranyl coprecipitated with calcite. The luminescence and XAFS data for the method I calcite (pH 8.2) show a local uranyl structure similar to that previously identified (Reeder et al., 2000). This was interpreted as containing dominantly five equatorial oxygens on the basis of the 2.33 Å U-O_{eq} distance, which is consistent with a CN value of 5 and thus at least one monodentate CO_3 group. However, the errors in the equatorial CN values determined by XAFS are approximately ± 1 and by themselves do not permit distinction between CN 5 and 6. The U-O_{eq} distance (2.33–2.34 Å) is approximately 0.1 Å shorter than the U-O_{eq} distance of the dominant aqueous species in the growth solution, $UO_2(CO_3)_3^{4-}$ (2.43 Å; Clark et al., 1995), in which all carbonates are in bidentate coordination.

The interpretation of equatorial coordination number on the basis of the average equatorial distance finds support from a survey of uranyl-containing crystal structures by Burns et al. (1997). The most common style of equatorial coordination of the UO_2 unit by carbonate ligands is with three CO_3 groups in bidentate coordination and approximately coplanar. The U-O_{eq} distance in well refined crystal structures with this coordination is typically 2.42 to 2.44 Å. The equatorial coordination number in rutherfordine (UO_2CO_3) is also six, but with two bidentate and two monodentate CO_3 groups. In rutherfordine, the average

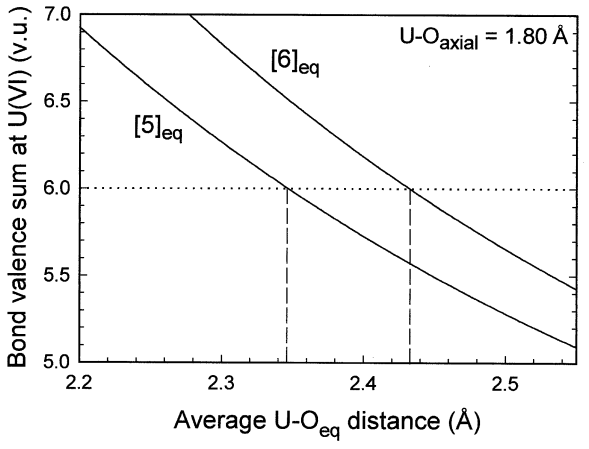

Fig. 11. Calculated curves showing the dependence of the bond valence sum at U(VI) on the average U-O_{eq} distance for five and six equatorial oxygens (at constant U-O_{ax} distance), based on the bond valence parameters from Burns et al. (1997). The vertical lines, which intersect the curves at a valence sum of six, show that a difference between an equatorial coordination number of five and six oxygens corresponds to a difference in average U-O_{eq} of approximately 0.09 Å.

U-O_{eq} distance is 2.48 Å, and the U-O_{eq} distance for the monodentate CO_3 groups is intermediate between bidentate U-O_{eq} distances (Finch et al., 1999). Uranyl carbonate crystal structures with 5 equatorial oxygens are comparatively rare; roubaultite ($Cu_2(UO_2)_3(CO_3)_2O_2(OH)_2{\cdot}4H_2O$) and bijvoetite-(Y) $\{[Y_8(H_2O)_{25}(UO_2)_{16}O_8(OH)_8(CO_3)_{16}](H_2O)_{14}\}$ are the only examples for which structures have been determined. These minerals contain both pentagonal and hexagonal bipyramidal coordination of U(VI) and hence offer comparisons of average equatorial bond distances. In roubaultite, the mean U-O_{eq} distances are 2.35 and 2.44 Å, respectively, for five and six equatorial oxygens (Ginderow and Cesbron, 1985). In bijvoetite-(Y) a similar difference in mean U-O_{eq} distances is found: 2.37 and 2.46 Å, respectively, for the pentagonal and hexagonal bipyramids (Li et al., 2000). The consistent difference of 0.09 Å primarily reflects the number of equatorial oxygens.

Relationships between bond length and coordination number are well established (e.g., Shannon and Prewitt, 1969) and have been formalized in bond valence theory (Brown, 1981). Burns et al. (1997) have recently redetermined bond valence parameters for U(VI)-O coordination from more than 100 well refined crystal structures. Figure 11 shows the dependence of the bond valence sum at U(VI) on the average distance for five and six equatorial oxygens (at constant U-O_{ax}). As expected the curves are offset reflecting the difference in average U-O_{eq} distance, with most common values of 2.34 and 2.43 Å, respectively, for CN 5 and 6. Whereas small deviations from these absolute values are certainly expected depending on the coordination of the oxygen ligands, the difference itself reflects the influence of CN on bond length. This systematic relationship should be useful for determining equatorial coordination number where disorder in the equatorial shell is evident and fitting of XAFS data yields only an average equatorial distance, as with the present data.

Therefore, the average equatorial distance of 2.33 Å in the method I calcite is consistent with a significant fraction (perhaps a majority) of the U(VI) absorbers having an equatorial coordination by five oxygens. The absence of backscattering from atoms beyond the carbon shell is consistent with static disorder of carbonate groups in which rotation or twisting has reduced or eliminated backscattering from distal oxygens. Such disorder could result in multiple orientations of the uranyl carbonate unit such that backscattering from near Ca atoms would also be minimal.

For the method II calcite, the luminescence results indicate that at least two distinct local coordination environments exist for the uranyl. One is essentially the same as that found in the method I calcite. The second type of coordination appears to be the same as the uranyl coordination in aragonite, i.e., the triscarbonato species, with all bidentate CO_3 groups and equatorial coordination number six. It is not possible to determine the relative proportion of these species in the calcite from luminescence spectra because their relative emission quantum yields are unknown.

The results of the XAFS fitting represent an average over all uranium local environments in the calcite. Depending on their relative proportions, the fit results may not depict any one particular uranyl environment unless it is so dominant that contributions from less abundant species are insignificant. Nevertheless, the fit results do suggest some constraints on the equatorial coordination for the method II uranyl-containing calcite. The average U-O_{eq} distance of 2.36 Å is nearer to the U-O_{eq} distance in the method I calcite (2.33 Å) than in aragonite (2.43 Å). Based on the previous discussion, this would suggest that the greater proportion of the U absorbers have five equatorial oxygens. But the weak contribution from distal oxygens in the method II calcite is consistent with a component of a triscarbonato-like species.

Finally, we note that the shoulder in the XANES spectrum for the method II uranyl-containing calcite is intermediate in importance between those for the method I calcite and aragonite. Although this is consistent with the interpretation that a "mixture" of these species exists in the method II calcite, it also raises the question of whether the equatorial coordination contributes to this feature, which has been interpreted as arising from multiple scattering within the linear O=U=O moiety.

4.2. Uranyl Incorporation into Calcite

As noted previously, the aqueous speciation calculations suggest that $UO_2(CO_3)_3^{4-}$ is the dominant uranyl species in both solutions. This species has six equatorial oxygens. The uranyl species in the method I calcite and what we interpret to be the more abundant of two uranyl species in the method II calcite both have an equatorial CN of 5. This difference indicates that a change in the equatorial coordination must have occurred during incorporation into the calcite. Reeder et al. (2000) noted that it might be as simple as one CO_3 ligand partially twisting off, changing from bidentate to monodentate linkage. However, more complex changes in equatorial coordination can also be envisioned, including loss of one or more CO_3 ligands and completion of equatorial CN 5 by oxygens from existing CO_3 groups in the calcite structure. The mechanism of coordination change remains speculation.

The additional finding of a minor triscarbonato species in the

method II calcite implies that this change in equatorial coordination is not necessarily effected for all incorporated uranyl species. The cause for a small amount of the triscarbonato species being incorporated should relate to differences in the crystal growth conditions between the two methods. The factors responsible remain undetermined at this point, but might include growth rate and details of the surface structure.

4.3. Significance of Site-selective Incorporation

The other major finding of this work is that structural aspects of the calcite growth surface exert a significant control on the magnitude of U(VI) uptake during coprecipitation. This is demonstrated by the growth step-selective incorporation on method II calcite $(10\bar{1}4)$ surfaces containing polygonized growth spirals. This surface structural control is consistent with previous observations of differential uptake of metal cations and complex anions according to growth step structure (cf. Reeder, 1996; Reeder and Rakovan, 1999). The pattern of preferential incorporation in the steps composing the a' and b' vicinals (relative to the a and b vicinals) agrees with the pattern observed for Mg^{2+}, Mn^{2+}, Co^{2+}, Cd^{2+}, and BO_3, but is opposite to the preference exhibited by Sr^{2+}, Ba^{2+}, Zn^{2+}, and anions SO_4^{2-} and SeO_4^{2-} (Staudt et al., 1994; Paquette and Reeder, 1995; Reeder, 1996; Hemming et al., 1998). The cause of the differential uptake has been attributed to differences in coordination geometry of the sites within the nonequivalent growth steps. It is easy to visualize site preferences for individual aquo ions (e.g., Sr^{2+}, Mn^{2+}, etc.), but not necessarily for the relatively large uranyl carbonate species with a complex geometry. One important consequence of this site- and step-selective uptake is that the relative proportion of the nonequivalent sites and/or steps exposed on a particular calcite surface will strongly influence the overall uptake behavior, perhaps by as much as a factor of ten. This raises the interesting prospect of treating or modifying the calcite surface to increase the fraction of the favorable sites/steps to enhance uranyl (or any metal) uptake.

Comparison of the polarized XANES spectra from adjacent, nonequivalent vicinals fails to suggest any discernible differences in local coordination of the uranyl in the different regions of the method II calcite, beyond the obvious difference in concentration. Hence, we conclude that the surface mechanism resulting in differential uptake appears not to influence the local coordination in terms of the different surface sites. Even so, it would seem likely that the coordination change associated with incorporation probably occurs at the surface, but further insight must await studies of uranyl adsorption. The uranyl unit has strong linear dichroism, and previous experimental studies have shown differences in L_3-edge XANES depending on the orientation of the uranyl unit relative to the polarization vector (Hudson et al., 1996). Hence, the lack of any observable difference in the polarized XANES spectra for the different orientations of the crystal relative to the polarization vector may indicate that there is no uniform or dominant orientation of the O=U=O moiety within the method II calcite single crystals. This would be consistent with the presence of multiple species, as shown by the luminescence, and with the apparent disorder beyond the first equatorial shell, as shown by the XAFS.

5. CONCLUSIONS

The findings of this study suggest that prediction of the fate of U(VI) bound with calcite is complicated by several factors. Solution chemistry influences aspects of crystal growth that, in turn, control the incorporation of uranyl species into calcite. This control is apparently associated with properties of the surface. Multiple uranyl species exist in the calcite grown from the high ionic strength solution at pH 7.6, whereas a single species dominates the calcite grown at pH 8.2 at lower ionic strength. In the samples studied, uranyl incorporation is accompanied by a change from bidentate to monodentate coordination for at least a fraction of the CO_3 ligands involved. In contrast, no similar change in coordination has been found to occur during incorporation into aragonite, in which the uranyl coordination is nearly identical to that in the aqueous solution, i.e., the triscarbonato species. It is worth noting that the equatorial coordination change for uranyl incorporation into calcite, and the absence of such a change for incorporation into aragonite, may explain the preferential uptake of uranyl by the latter (cf. Reeder et al., 2000).

The findings also have potentially important implications for sequestration and remobilization of U(VI) in calcite. It is likely that geometries of the uranyl species in the calcite require significant disruption of the local structure. This suggests that uranyl incorporation should increase the solubility of calcite. Reeder et al. (2000) speculated that the observed disorder beyond the shell of equatorial oxygens probably reflects a less stable coordination environment for U(VI) than in uranyl compounds or even aragonite, where its coordination geometry is well defined. Our previous experiments have shown that significant amounts of uranium can be taken up by coprecipitation with calcite (up to 1900 ppm) and aragonite (up to 10000 ppm). In natural calcites, uranium concentrations rarely exceed 10 ppm. Of course, these lower concentrations in part reflect natural abundances in crystallizing fluids. Yet the uranium seems to be effectively immobilized within the calcite structure for millions of years, implying that the local coordination of uranium in natural calcite is structurally stable. Sturchio et al. (1998) showed this to be true for U(IV) in natural calcite, where the U^{4+} ion occupies the Ca position with minimal distortion. Similar characterization is needed for U(VI) in natural calcite, particularly in view of the expected disruption of the local coordination around UO_2^{2+}. It is possible that the coordination of uranyl observed in our coprecipitation experiments does not reflect the final state over longer time periods. That raises the possibilities of dissolution, selective loss, and structural transformation, any of which could influence remobilization of uranium.

Acknowledgments—Funding for this work was provided by DOE grant DE-FG07-99ER15013 through the Environmental Management Science Program and by NSF grant EAR9706012. C.D.T. and D.E.M. received support from the LANL Laboratory Directed Research and Development Program. We thank beamline personnel at X11A (NSLS), X26A (NSLS), and 20-ID-B (APS) for their assistance with various experimental aspects of this work. A.R. Felmy kindly made available his database with estimated Pitzer equation parameters for calculation of aqueous uranyl speciation. We thank E. Curti and two anonymous reviewers, whose comments improved the final version.

Associate editor: J. D. Rimstidt

REFERENCES

Allison J. D., Brown D. S. and Novo-Gradac K. J. (1991) MINTEQA2, A geochemical assessment data base and test cases for environmental systems: Vers. 3.0 user's manual. Report EPA/600/3–91/-21. Athens, GA, U.S. E.P.A.

Amayri S., Bernhard G. and Nitsche H. (1999) Solubility of $Ca_2[UO_2(CO_3)_3]\cdot 10\ H_2O$, liebigite. *Ann. Report 1998 Institute of Radiochemistry,* Forschungszentrum Rossendorf, FZR-**247,** p. 12.

Bernhard G., Geipel G., Brendler V. and Nitsche H. (1996) Speciation of uranium in seepage waters of a mine tailing pile studied by time-resolved laser-induced fluorescence spectroscopy (TRLFS). *Radiochim. Acta* **74,** 87–91.

Broecker W. S. (1963) A preliminary evaluation of uranium series inequilibrium as a tool for absolute age measurements on marine carbonates. *J. Geophys. Res.* **68,** 2817–2834.

Brown I. D. (1981) The bond-valence method: An empirical approach to chemical structure and bonding. In *Structure and Bonding in Crystals,* (eds. M. O'Keefe and A. Navrotsky) Vol. 2, pp. 1–30. Academic Press, New York.

Burns P. C., Ewing R. C. and Hawthorne F. C. (1997) The crystal chemistry of hexavalent uranium: Polyhedron geometries, bond-valence parameters, and polymerization of polyhedra. *Can. Min.* **35,** 1551–1570.

Carroll S. A., Bruno J., Petit J-C. and Dran J-C. (1992) Interaction of U(VI), Nd, and Th(IV) at the calcite-solution interface. *Radiochim. Acta* **58/59,** 245–252.

Cheng L., Sturchio N. C. and Bedzyk M. J. (2000). Local structure of Co^{2+} incorporated at the calcite surface: An x-ray standing wave and SEXAFS study. *Phys. Rev.* **B61,** 4877–4883.

Clark D. L., Hobart D. E., and Neu M. P. (1995) Actinide carbonate complexes and their importance in actinide environmental chemistry. *Chem. Rev.* **95,** 25–48.

Clark D. L., Conradson S. D., Donohoe R. J., Keogh D. W., Morris D. E., Palmer P. D., Rogers R. D. and Tait C. D. (1999) Chemical speciation of the uranyl ion under highly alkaline conditions. Synthesis, structures, and oxo ligand exchange dynamics. *Inorg. Chem.* **38,** 1456–1466.

Curti E. (1999) Coprecipitation of radionuclides with calcite: estimation of partition coefficients based on a review of laboratory investigations and geochemical data. *Appl. Geochem.* **14,** 433–445.

Davis J. A., Fuller C. C. and Cook A. D. (1987) A model for trace metal sorption processes at the calcite surface: Adsorption of Cd^{2+} and subsequent solid solution formation. *Geochim. Cosmochim. Acta* **51,** 1477–1490.

Felmy A. R. (1995) GMIN, a computerized chemical equilibrium program using a contrained minimization of the Gibbs free energy: Summary report. *Chemical Equilibirum and Reaction Models, Soil Sci. Soc. Am., Spec. Publ.* **42,** 377–407.

Felmy A. R. and Rai D. (1999) Application of Pitzer's equations for modeling the aqueous thermodynamics of actinides species in natural waters: A review. *J. Sol. Chem.* **28,** 533–553.

Finch R. J, Cooper M. A., Hawthorne F. C. and Ewing R. C. (1999) Refinement of the crystal structure of rutherfordine. *Can. Min.* **37,** 929–938.

Geipel G., Reich T., Brendler V., Bernhard G. and Nitsche H. (1997) Laser and X-ray spectroscopic studies of uranium-calcite interface phenomena. *J. Nucl. Mater.* **248,** 408–411.

Ginderow P. D. and Cesbron F. (1985) Structure de la roubaultite, $Cu_2(UO_2)_3(CO_3)_2O_2(OH)_2\cdot 4H_2O$. *Acta Cryst.* **C41,** 654–657.

Gratz A. J., Hillner P. E. and Hansma P. K. (1993) Step dynamics and spiral growth on calcite. *Geochim. Cosmochim. Acta* **57,** 491–495.

Grenthe I., Fuger J., Konings R. J. M., Lemire R. J., Muller A. B., Nguyen-Trung C. and Wanner H. (1992) Chemical Thermodynamics of Uranium. North-Holland, Amsterdam.

Hall P. O. and Aller R. C. (1992) Rapid, small-volume flow-injection analysis for ΣCO_2 and NH_4^+ in marine and fresh waters. *Limnol. Oceanogr.* **37,** 1113–1119.

Hemming N. G., Reeder R. J. and Hart S. R. (1998) Growth-step-selective incorporation of boron on the calcite surface. *Geochim. Cosmochim. Acta* **62,** 2961–2968.

Hudson E. A., Rehr J. J. and Bucher J. J (1995) Multiple-scattering calculations of the uranium L_3- edge x-ray-absorption near-edge structure. *Phys. Rev.* **B52,** 13815–13826.

Hudson E. A., Allen P. G., Terminello L. J., Denecke M. A. and Reich T. (1996) Polarized x-ray absorption spectroscopy of the uranyl ion: Comparison of experiment and theory. *Phys. Rev.* **B54,** 156–164.

Kato Y., Meinrath G., Kimura T., and Yoshida Z. (1994) A study of U(VI) hydrolysis and carbonate complexation by time-resolved laser-induced fluorescence spectroscopy (TRLFS). *Radiochim. Acta* **64,** 107–111.

Kitano Y. and Oomori T. (1971) The coprecipitation of uranium with calcium carbonate. *J. Oceanogr. Soc. Jpn.* **27,** 34–42.

Li Y. P., Burns P. C., and Gault R. A. (2000). A new rare-earth-element uranyl carbonate sheet in the structure of bijvoetite-(Y). *Can. Mineral.* **38,** 153–162.

Mason C. F. V., Turney W. R. J. R., Thomson B. M., Lu N., Longmire P. A., and Chisholm-Brause C. J. (1997) Carbonate leaching of uranium from contaminated soils. *Env. Sci. Tech.* **31,** 2707–2711.

Meece D. E. and Benninger L. K. (1993) The coprecipitation of Pu and other radionuclides with $CaCO_3$. *Geochim. Cosmochim. Acta* **57,** 1447–1458.

Meinrath G. (1998) Aquatic chemistry of uranium. *Freiberg On-line Geoscience* **1,** 1–100.

Min G. R., Edwards R. L., Taylor F. W., Recy J., Gallup C. D., and Beck J. W. (1995) Ann. cycles of U/Ca in coral skeletons and U/Ca thermometry. *Geochim. Cosmochim. Acta* **59,** 2025–2042.

Mucci A. and Morse J. W. (1990) Chemistry of low-temperature abiotic calcites: Experimental studies on coprecipitation, stability and fractionation. *Aquatic Sci.* **3,** 217–254.

Paquette J. and Reeder R. J. (1995) Relationship between surface structure, growth mechanism, and trace element incorporation in calcite. *Geochim. Cosmochim. Acta.* **59,** 735–749.

Parkhurst D. L. (1995) User's guide to PHREEQC—a computer program for speciation, reaction- path, advective-transport, and inverse geochemical calculations. *U. S. G. S. Water Res. Inv. Rept.* 95–4227.

Plyasunov A., Fanghänel T., and Grenthe I. (1998) Estimation of Pitzer equation parameters for aqueous complexes. A case study of uranium at 298.15 K and 1 atm. *Acta Chemica Scand.* **52,** 250–260.

Reeder R. J. (1996) Interaction of divalent cobalt, zinc, cadmium, and barium with the calcite surface during layer growth. *Geochim. Cosmochim. Acta.* **60,** 1543–1552.

Reeder R. J. and Rakovan J. (1999) Surface structural controls on trace element incorporation during crystal growth. In *Growth, Dissolution and Pattern Formation in Geosystems* (eds. B. Jamtveit and P. Meakin), p. 143–162. Kluwer Academic.

Reeder R. J., Nugent M., Lamble G. M., Tait C. D., and Morris D. E. (2000). Uranyl incorporation into calcite and aragonite: XAFS and luminescence studies. *Env. Sci. Tech.* **34,** 638–644.

Ressler T. (1997) WinXAS: A new software package not only for the analysis of energy- dispersive XAS data. *J. Physique IV.* **7,** C2–269.

Rimstidt J. D., Balog A. and Webb J. (1998) Distribution of trace elements between carbonate minerals and aqueous solutions. *Geochim. Cosmochim. Acta* **62,** 1851–1863.

Russell A. D., Emerson S., Nelson B. K., Erez J., and Lea D. W. (1994) Uranium in formaniniferal calcite as a recorder of seawater uranium concentrations. *Geochim. Cosmochim. Acta* **58,** 671–681.

Shannon R. D. and Prewitt C. T. (1969) Effective ionic radii in oxides and fluorides. *Acta Cryst.* **B25,** 925–946.

Shen G. T. and Dunbar, R. B. (1995) Environmental controls on uranium in reef corals. *Geochim. Cosmochim. Acta.* **59,** 2009–2024.

Staudt W. J., Reeder R. J., and Schoonen M. A. A. (1994) Surface structural controls on compositional zoning of SO_4^{2-} and SeO_4^{2-} in synthetic calcite single crystals. *Geochim. Cosmochim. Acta.* **58,** 2087–2098.

Stipp S. L., Hochella M. F., Parks G. A. and Leckie J. O. (1992) Cd^{2+} uptake by calcite, solid-state diffusion, and the formation of solid solution: Interface processes observed with near- surface sensitive techniques (XPS, LEED, and AES). *Geochim. Cosmochim. Acta.* **56,** 1941–1954.

Sturchio N. C., Chiarello R. P., Cheng L., Lyman P. F., Bedzyk M. J. and Baer D. R. (1997) Lead adsorption at the calcite-water interface: Synchrotron X-ray standing wave and X-ray reflectivity studies. *Geochim. Cosmochim. Acta.* **61,** 251–263.

Sturchio N. C., Antonio, M. R., Soderholm L., Sutton S. R., and Brannon J. C. (1998) Tetravalent uranium in calcite. *Science* **281,** 971–973.

Swart P. K. and Hubbard J. A. E. B. (1982) Uranium in scleractinian coral skeletons. *Coral Reefs.* **1,** 13–19.

Sylwester E. R., Hudson E. A. and Allen P. G. (2000). The structure of uranium (VI) sorption complexes on silica, alumina, and montmorillonite. *Geochim. Cosmochim. Acta* **64,** 2431–2438.

Teng H. H., Dove P. M., Orme C. A. and De Yoreo J. J. (1998) Thermodynamics of calcite growth: Baseline for understanding biomineral formation. *Science* **282,** 724–727.

Tesoriero A. J. and Pankow J. F. (1996) Solid solution partitioning of Sr^{2+}, Ba^{2+}, and Cd^{2+} to calcite. *Geochim. Cosmochim. Acta.* **60,** 1053–1063.

Thompson H. A., Brown G. E. and Parks G. A. (1997) XAFS spectroscopic study of uranyl coordination in solids and aqueous solution. *Am. Mineral.* **82,** 483–496.

Xu N., Hochella M. F., Brown G. E. and Parks G. A. (1996) Co(II) sorption at the calcite-water interface: I. X-ray photoelectron spectroscopic study. *Geochim. Cosmochim. Acta* **60,** 2801–2815.

Zabinsky S. I., Rehr J. J., Ankudinov A., Albers R. C. and Eller M. J. (1995) Multiple-scattering calculations of X-ray absorption spectra. *Phys. Rev.* **B52,** 2995–3009.

Zachara J. M., Cowan C. E. and Resch C. T. (1991) Sorption of divalent metals on calcite. *Geochim. Cosmochim. Acta* **55,** 1549–1562.